PREPRINT UCRL-82426, Rev. 1

CONF-790393--1

Lawrence Livermore Laboratory

PHYSICS OF INERTIAL CONFINEMENT PELLETS

William C. Mead

July 9, 1979

MASTER

Prepared for the American Physical Society Meeting, March 19-23, 1979, Chicago, Illinois.

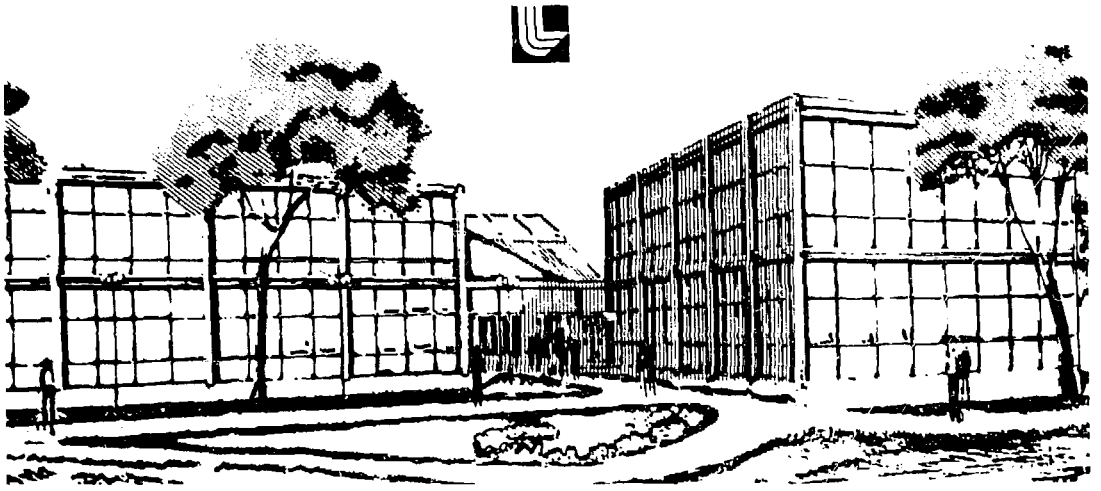

PHYSICS OF INERTIAL CONFINEMENT PELLETS*

William C. Mead
Lawrence Livermore Laboratory
Livermore CA 94550

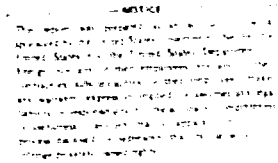

Viewgraphs i & ii

This talk will be in four parts. The first section will be an overview of inertial confinement fusion pellet physics. This will serve as an orientation to those who are unfamiliar with ICF concepts. The second section is a discussion of current estimated ICF driver requirements and a couple of pellet examples. Next I will go into the physics of driver/plasma coupling for two drivers which are being considered, namely a laser driver and a heavy ion accelerator driver. Finally, I will have a few brief things to say about progress towards inertial confinement fusion that has been made using laser drivers in target experiments to date.

The work discussed here is the result of the efforts of many people. I am particularly grateful to J. H. Nuckolls, J. D. Lindl, W. L. Kruer, and R. O. Bangerter for their contributions.

*Work performed under the auspices of the U.S. Department of Energy by the Lawrence Livermore Laboratory under contract No. W-7405-ENG-48.

Viewgraph #1

Inertial confinement energy is released during thermonuclear burn of compressed fuel.[1,2] The performance of an ICF pellet depends on a variety of physical processes. Energy is delivered to the target by the driver and couples into the plasma. The energy is then thermalized and transported into high density material to what is called the ablation front. Here, heated dense matter blows off to lower density. depositing momentum in the remaining material which is accelerated inward. compressing the DT fuel. When the fuel reaches sufficient density and temperature. thermonuclear burn begins and. if all works well. the thermonuclear energy output is sufficient to provide significant net energy.

Viewgraph #2

The seeds of fusion power were planted years ago by the designer of the universe. The easiest nuclei to fuse are deuterium and tritium. which join to produce an alpha particle and a neutron. releasing a net binding energy of 17.6 MeV per reaction. The coulomb repulsion of the nuclei involved causes the cross section for the process to decrease to vanishingly small values at low reaction temperatures. At DT plasma temperatures of 10 keV or above. the ions at energies of 30-50 keV have a reaction cross section which is quite large.

Viewgraph #3

Inertial confinement is effective when the thermonuclear burn time is

significantly greater than the disassembly time for the fuel. The relative thermonuclear reaction rate in a blob of hot DT is proportional to the density of deuterium times the density of the tritium times $\langle\sigma v\rangle$, the velocity-averaged cross section. The burn continues until a spherical rarefaction wave disassembles the burning DT by causing a reduction in both the density and temperature. A figure of merit for the success of confinement is the ρR product of the burning fuel and the burn efficiency ϕ is proportional to $\rho R/(\rho R + 6)$. Note that compression helps increase the ρR for a given mass of DT fuel.

Viewgraph #4

The thermonuclear energy output from DT burn can be vastly greater than the energy required to compress it. At a burn efficiency of 40% the energy released by thermonuclear burn is nearly four orders of magnitude higher than the energy required to assemble the matter in its Fermi degenerate state at density 600 g/cm^3. This is a fortunate state of affairs but there are two problems remaining. First, the DT will not ignite at its degenerate temperature of .1 keV; and, second, a low-isentrope compression technique is needed.

Viewgraph #5

Central ignition combined with propagating burn are the keys to high gain. If a central region of fuel having ρR of .5 g/cm^2 can be brought to 10 keV, the alpha particle products of the burn of the central portion provide sufficient energy to ignite a surrounding fuel mass three times as large as the initial burning mass.

Viewgraph #6

Spherical implosion is useable to deliver the phenomenal energy density for assembling inertially-confined fuel. Heating the outside of an ablator shell causes a pressure peak, which accelerates matter both inward and outward. This essentially is a spherical rocket, with its thrust outward, and it propels the fuel and inner ablator inward with the velocity given approximately by the rocket equation:

$$v(t) = \frac{P_A}{\dot{m}} \ln\left[\frac{m_i}{m(t)}\right] .$$

Viewgraph #7

The rocket thrust is determined by the heat flux delivered to the ablation front. Here we consider the deposition of laser beams near the critical density surface surrounding the pellet. Energy is deposited near critical and transported by electron thermal conduction to the ablation surface. The flux reaching the ablation surface determines the ablation pressure:

$$P_A \simeq 1.6 \times 10^4 \, f^{1/3} \left(\eta_c \eta_T I_D \, \frac{\lambda_{Nd}}{\lambda_D}\right)^{2/3}$$

Here f is the effective thermal flux limit reduction, and η_C and η_T are the efficiencies for laser coupling and subsequent transport of energy into the ablation surface. λ_{Nd} = 1.06 μm is the wavelength of a Nd-glass laser. I_D and λ_D are the driving laser intensity and wavelength.

Viewgraph #8

We now have the zero-order tools to complete a first-cut inertial confinement fusion pellet design.[3] We need to attain a final energy density of 2×10^7 J/g in the fuel, which requires an implosion velocity of 2×10^7 cm/sec. We will consider a shell of 3 mm inside diameter, which then would have an implosion time of 3×10^{-8} sec. We take a fuel mass of 1 milligram of DT and use the rocket equation to find the optimum ablator mass to propel this payload. The driving pressure we need is then 7×10^{12} ergs/cm^3. We assume a 1/4-micron laser. Let us assume a coupling efficiency of .7, a thermalization and transport efficiency of .5, and an electron thermal flux limit factor of .1. From the transport equation we obtain the peak intensity of the driver, of approximately 2×10^{13} W/cm^2, and a peak driver power of about 40 TW, requiring a driver energy of 0.5 MJ. The yield of this assembled DT mass is about 140 MJ of TN energy, for a pellet gain of about 300. This must be our lucky day!

Viewgraph #9

To these basics a few higher order considerations need to be added.

Driver plasma coupling may not be so simple. Pulse shaping details are needed to set and maintain the proper isotrope for fuel and ignition mass. Timing is a delicate matter. Preheat, fluid instabilities and spherical symmetry of the implosion are all quantitatively potential limitations to the implosion system performance.[4,5,6] These, though important, are beyond the scope of this presentation.

ICF Driver Requirements, Pellet Examples

Viewgraph #10

Physical characteristics of proposed ICF drivers cover a wide range and involve a wide variety of interactions. Just to illustrate the spread in characteristics, this figure shows the values of two parameters, chosen somewhat randomly. The first is the effective wavelength ($\lambda = h/p$, for particle beam drivers). The laser drivers in use and proposed are shown at their respective wavelengths. This indicates roughly the "deflectability" of the particles, with higher momentum (shorter wavelength) particles requiring a greater momentum transfer to produce a given angular deflection.

The second parameter is $(p/Z)/(Z/E_k)$, an indicator of the tendency of a beam of given energy per unit area to deflect in its own magnetic field.

Viewgraph #11

The interaction length is a parameter of considerable interest to ICF

pellet performance. The band shaded over parameter space is a rough optimum from a pellet point of view. Ranges longer than .2 g/cm^2 increase the required driving energy. Ranges shorter than .02 g/cm^2 increase reliance on electron transport to carry the energy to the ablation surface. Note that other factors could somewhat shift the optimum driver/pellet combination.

The interaction ranges of charged particles in ICF plasmas are plotted for 1-10 MeV e^-, 1-10 MeV H^+ ions, and 2-20 GeV U^+ ions. In order to put lasers on the same plot, the model density profile shown was used. Changes in the assumed profile would shift the lasers somewhat relative to the particles.

The position of the CO_2 laser is shown as a band to indicate possible changes due to use of different irradiation intensities. The lefthand edge corresponds to interaction at $n_e \simeq 10^{20}$ cm^{-3} with $T_{HOT} \simeq 10$ keV conditions roughly appropriate for $I \simeq 10^{14}$ W/cm^3. The band to the right assumes higher intensity irradiation with energy deposited into higher electron energies which have longer range. The generally Maxwellian shape of laser generated hot electrons provides significant numbers of very energetic electrons (preheat-generating) with ranges long relative to those of the average electrons (drive-generating). This broad range of interaction lengths under given irradiation conditions can make preheat shielding a significant difficulty under some conditions.

Viewgraph #12

To use inertial confinement fusion as a source of commercial

electricity, the product of the pellet gain and the driver efficiency must exceed 10.

Viewgraph #13

Our estimates for the required ICF driver characteristics are shown in this slide.[7] A driver energy of 1-3 MJ, with power of 100 400 TW and capable of depositing between 10^7-10^8 J/gm is required. A wavelength/voltage limitation is imposed by coupling limits for drive and preheat to the ICF pellet.

Further, the driver efficiency must be a minimum of 1-2%, preferably toward 10%. In any case, the product of the pellet gain and the drive efficiency must exceed 10 The driver must be able to fire repetitively at 1-20 Hz, must focus across a reaction chamber about 5 meters radius to 5 millimeters spot diameter. This latter group of requirements arises fom reactor design considerations.

Viewgraph #14

Next we consider as an example, a 1 MeV electron beam driven, single-shell target using massive ablator and a dense pusher to achieve gain of 25 at 6 MJ and 1200 TW input.[8] The broad deposition profile of electron beams and the sizeable amount of bremsstrahlung radiation with long mean-free-path mean that preheat is a limitation. On the other hand. long density gradients imply that fluid instabilities are relatively benign.

Viewgraph #15

Next we look at a 6.5 MeV proton-beam driven target using a tamped pusher to compress the fuel.[9] This target has calculated gain ~ 90 at 1.3 MJ and 250 TW input. In this design the ions penetrate the high-Z tamper with relatively little deposition, then deposit their energy in quite a short distance in the low-Z pusher surrounding the DT fuel. High performance depends upon precision pulse shaping for this target.

Driver-Plasma Coupling

In this section we discuss driver-plasma interaction for two drivers under consideration. First, I will talk about laser-plasma coupling, then heavy ion plasma coupling.

Viewgraph #16

Laser absorption can occur by processes in two general categories First, collisional heating by inverse bremsstrahlung is most effective at low intensities and long pulse length. It produces background or thermal heating. Second, collective absorption, in which a light wave excites plasma waves which in turn heat the particles of the plasma, is dominant at high intensities and short pulse lengths.[10] In general, collective heating produces relatively small numbers of very energetic superthermal electrons.

Viewgraph #17

This viewgraph illustrates the various collective processes which can absorb or scatter laser light incident on a plasma density profile. Of particular interest are resonance absorption and parametric instabilities which absorb light at the critical density. In the underdense plasma, stimulated Brillouin scattering can backreflect the incident laser light on its way to the critical surface. Filamentation can cause the light to form intense narrow channels which modify the absorption and heating characteristics of the laser light. Note also that magnetic fields and ion turbulence can be created near the critical density surface which may inhibit the electron thermal conduction from the region of energy deposition and heating into the ablation surface. I will now deal with each of these four areas in a little more detail.

Viewgraph #18

Resonance absorption is the simplest example of heating via plasma waves.[11,12] The laser light is obliquely incident with its polarization vector parallel to the plane of incidence. A component of the laser electric field oscillates electrons along the density gradient, causing a charge density variation which resonantly drives an electron plasma wave near the critical density. Calculations[13 14] show typically about 30% absorption into hot electrons, with characteristic temperatures in the range of 5-150 keV depending on the laser intensity and wavelength.

Viewgraph #19

These hot electron temperatures are reasonably quantitative agreement with temperatures inferred from x-ray energy ratio measurements on a variety of target experiments.[15,16]

Viewgraph #20

Computer calculations predicted the principal features of high intensity laser light absorption. This viewgraph shows the absorption fraction as a function of angle of incidence for p- and s-polarization. Note that only p-polarization absorption corresponding to resonant absorption on a steepened density profile. 60% of the absorption is accounted for by the resonance absorption and the remainder can be attributed to other physical processes.

Viewgraph #21

Stimulated Brillouin scattering can reflect laser light below the critical density.[17,18] It is produced by coupling between an incoming high frequency electromagnetic wave and a low frequency ion wave in theunderdense plasma. The process grows from ion density perturbations in the plasma which couple to the laser electric field, producing an oscillating current in the plasma which in turn causes re-radiation of light propagating in the opposite direction. The beating between the reflected and the incident wave in turn generates a low-frequency electric field which drives the ion perturbations to larger amplitude. This

feedback process gives an instability which grows exponentially with time and space as the laser light propagates into the plasma.

Viewgraph #22

Plasma simulations have predicted sizeable Brillouin scatter in long pulse length experiments. Shown here are measurements at 5×10^{16} W/cm^2 on low-Z disk targets irradiated at 80 and 200 picoseconds.[15,18] The decrease in the absorption fraction is attributed to increase in reflectivity due to Brillouin scattering as the scale length of the plasma gets longer.

Viewgraph #23

Brillouin scattering heats the ions and subsequently the ion waves become damped. This viewgraph shows a plot of ion phase space for a 1-D plasma simulation in which ion waves have been driven to nonlinear amplitudes and heated ions are being ejected at high velocity.[19]

Viewgraph #24

Stimulated backscatter can be sizeable in a large, underdense plasma. A theoretical model for Brillouin scattering in the heavily-damped regime[20] shows that the amount of Brillouin scattering increases as the plasma density over the critical density, the scale length over the wavelength, and the laser intensity.

Viewgraph #25

Laser light can [illegible] long wavelength, large focal spot experiments.[21,22] Filamentation due to the ponderomotive force and due to joule heating is above its convective growth threshold for typical high intensity laser plasma experiments. This can raise the intensity at the critical surface significantly.

Viewgraph #26

Higher laser intensity at the critical surface implies higher heated electron temperatures. Thermoelectric magnetic fields can form around the filament possibly affecting transport of energy.

Viewgraph #27

Experiments sometimes show signs of filament formation,[16] as illustrated by this picture of a high-Z plasma irradiated by the laser beam on the left of the figure. The pictures on the right are x-ray microscope images of the heated plasma with various energy windows and show clear formation of hot spots which correspond with intensity peaks in the incident laser beam.

Viewgraph #28

Electron transport may be reduced compared with free-streaming value[23] in hot laser-produced plasmas. Numerical modeling of various experiments suggests an effective flux reduction of the order of a factor

of 30, in order to obtain reasonable value for inverse bremsstrahlung absorption. ion expansion velocities. x-ray emission, spatial and spectral distributions.[15] and the heating depth for layered targets.[24,25]

Viewgraph #29

Magnetic fields may play a significant role in transport inhibition.[15,26,27] A magnetic field of a few megagauss can significantly reduce the transport of low energy electrons at densities about twice the neodymium critical density. Hot electrons can also be inhibited by even lower magnetic fields, however, the spatial extent of the field must be much larger than the cyclotron radius of the electrons in the magnetic field.

Viewgraph #30 - Summary of Laser-Plasma Coupling

Competition among processes is very important. This can lead to wide variations in the absorption and heating conditions. Major phenomena are collisional absorption, collective absorption into hot electrons, stimulated Brillouin scattering. filamentation. and inhibited transport. Experiments have suggested the existence of each of these. The coupling picture generally improves at shorter wavelengths and lower intensities.

Viewgraph #31

Now we turn to ion-beam/plasma coupling physics[28] and consider two classes of processes: atomic and nuclear. We will concentrate here on the slowing down of heavy ions in a plasma typical of ICF conditions.

Viewgraph #32

Energy loss of ions in matter primarily results from binary collisions with electrons. The electron kinetic energy is determined essentially by the impact parameter of the collision.

Viewgraph #33

The energy loss of an ion is calculated by integrating the differential cross section over appropriate limits. The minimum kinetic energy transfer is determined for solid matter by comparing the binding energy of the atomic electrons to the energy imparted by collision. In a plasma, the maximum impact parameter B_{MAX} and the minimum energy transfer T_{min} are determined by the Debye length

Viewgraph #34

For ICF applications we are interested in placing an upper limit on the range of an incident ion beam, since the driving energy required increases with the range. Consequently, it is of interest to derive a rigorous lower limit on T_{max}/T_{min}. This limit has the pleasing property of being not very much larger than the expected range in a plasma, and turns out to be tolerable for driving an ICF target.

Viewgraph #35

Thus, a rigorous lower limit on dE/dx can be set, based on relatively simple and secure assumptions.

Viewgraph #36

Energy conservation prevents significant acceleration or decceleration of ions by plasma electric fields during slowing down.

Viewgraph #37

This viewgraph illustrates the non-collective nature of the heavy-ion/plasma interaction.

Viewgraph #38

Electron preheat is not severe since the range of even the most energetic electrons is comparable to or less than the incident ion range.

Viewgraph #39

Now we turn to nuclear interactions, which represent wasted energy and are a possible source of preheat, but in fact are not a fundamental problem. From the estimated cross section for nuclear reactions of 3.1×10^{-24} cm^2 we expect a 93% survival rate for 20 GeV uranium ions incident on beryllium.

Viewgraph #40

Cold matter measurements of ion ranges confirm well-established theory. Deposition of high current heavy ion beams in plasmas has not yet been measured.

Viewgraph #41

In summary, the theory for cold matter ion stopping is well established. A rigorous upper limit on ion range is low enough to permit use of 5-10 GeV uranium to drive ICF targets. Preheat from heated electrons and nuclear reaction losses both appear tolerable.

This coupling picture looks attractive, indeed, but must meet the test of more detailed analysis and future experiments!

Progress Towards Inertial Confinement Fusion

Viewgraph #42

This is one version of the grand plan for inertial confinement fusion. Plotted is the inertial confinement quality product n against the DT ion temperature in keV. Reactor targets are required to operate in the upper righthand corner of this figure. The lower curve represents the use of exploding pusher targets to obtain high DT temperatures and significant thermonuclear yields with small laser drivers. The upper line corresponds to using small lasers to achieve low isentrope implosions to high DT densities while not achieving ignition conditions. The recent 50-100X liquid density implosion experiments are indicated here. As the designs reach 1000 X liquid density, effort turns toward achieving ignition conditions by raising the temperature of the DT fuel.

I would like to spend the remaining few minutes discussing the diagnosis of density in inertial confinement pellet experiments and putting the progress to date in perspective within the grand plan of ICF.

Viewgraph #43

Diagnosis of fuel density in a low-isentrope, moderate-to-high density implosion is difficult. One method applicable to some near-term experiments shown here is nuclear activation of Si in a glass pusher.[29] This measures the pusher ρR driving TN burn directly.

A simple model can be used to relate the pusher ρR to an average DT density. More detailed analysis can be done using computer modeling for the target dynamics. Improved diagnosis can be made by seeding the fuel with an appropriate element. This generally requires a higher yield - ρR performance level.

Viewgraph #44

Two methods are available for using line emission of Ar seed in the DT fuel. Calculations show that core temperatures of .5-.8 keV are sufficient to strip Ar to its H-like and He-like ionization states.[30] For targets fabricated using a glass mandrel, emission of the resonance lines around 3 keV is attenuated somewhat in passing out through the compressed SiO_2 pusher material. This can be kept tolerable by minimizing the initial thickness of glass. Stark broadening of x-ray lines of an argon seed material in the fuel allows deduction of the density. Theoretical calculations are used to relate the impact broadening to the density. This method is susceptible to opacity and doppler broadening of the x-ray lines, which can be a source of confusion. Use of a crystal spectrograph in conjunction with a pinhole allows formation of an x-ray image of argon seed material line emission on

REFERENCES UCRL-82426

1. J. Nuckolls, L. Wood, A. Thiessen, and G. Zimmerman, Nature (London) 239, 139 (1972).
2. J. H. Nuckolls in H. J. Schwarz and H. Hora, Laser Interaction and Related Plasma Phenomena, Vol. 3B, (New York, 1973), p. 399.
3. J. H. Nuckolls, R. O. Bangerter, J. D. Lindl, W. C. Mead, Y L. Pan, University of California Report UCRL-79373, Rev. 1 (1977), and European Conference on Laser Interaction with Matter, Oxford, England (1977).
4. W. C. Mead and J. D. Lindl, University of California Report UCRL-75877 (1974), and Bull. Amer. Phys. Soc., 19, 950 (1974).
5. J. D. Lindl and W. C. Mead, Phys. Rev. Lett. 34, 1273 (1975).
6. G. S. Fraley, W. P. Gula, D. B. Henderson, R. L. McCrory, R. C. Malone, R. J. Mason, and R L. Morse, Fifth I.A.E.A. Conference on Plasma Physics and Controlled Nuclear Fusion Research, Tokyo, Japan (1974), paper IAEA-CN-33/F5-5.
7. J. D. Lindl, R. O. Bangerter, and J. H. Nuckolls, private communication.
8. M J. Clauser and M. A. Sweeney, International Topical Conference on Electron Beam Research and Technology, Sandia Laboratories Report SAND 76-5122, Vol. I, 135 (1976).
9. R. O. Bangerter and D. J. Meeker, Univ. of Calif. Report UCRL-78474 (1976) and Bull. Amer. Phys. Soc. 21, 1196 (1976).

10. W. L. Kruer, R. A. Haas, W. C. Mead, D. W. Phillion, and V. C. Rupert, in Plasma Physics, Nonlinear Theory and Experiments, edited by H. Wilhelmson (Plenum, New York 1977), p. 64.

11. V. L. Ginzburg, The Properties of Electromagnetic Waves in Plasmas (Pergamon, New York, 1964).

12. J. P. Freidberg, R. W. Mitchell, R. L. Morse and L. F Rudsinski, Phys. Rev. Letters 28, 795 (1972).

13. K. G. Estabrook, E. J. Valeo and W. L. Kruer, Phys Fluids 18, 1151 (1975); E. J. Valeo and W. L. Kruer, Phys. Rev. Letters 33, 750 (1974).

14. D. W. Forslund, J. M. Kindel, K. Lee, E. L. Lindman and R. L. Morse, Phys. Rev. A 11, 679 (1975); J. M. Kindel, K. Lee, and E. L. Lindman, Phys. Rev. Letters 34, 134 (1975).

15. W. C. Mead, R. A. Haas, W. L. Kruer, D. W. Phillion, H. N. Kornblum, J. D. Lindl, D. R. MacQuigg, and V. C. Rupert, Phys. Rev. Lett. 37, 489 (1976); R. A. Haas, W. C. Mead, W. L. Kruer, D. W. Phillion, H. N. Kornblum, J. D. Lindl, D. MacQuigg, V. C. Rupert, and K. G. Tirsell, Phys. Fluids 20, 322 (1977).

16. H. D. Shay, R. A. Haas, W. L. Kruer, M. J. Boyle, D. W. Phillion, V. C. Rupert, H. N. Kornblum, F. Rainer, V. W. Slivinsky, L. N. Koppel, L. Richards, and K. G. Tirsell, Phys. Fluids 21, 1634 (1978).

17. B. I. Cohen and C. E. Max, Phys. Fluids 22, 1115 (1979).

18. D. W. Phillion, W. L. Kruer and V. C. Rupert, Phys. Rev. Lett. 39, 1529 (1977).

19. K. G. Estabrook, private communication (1979).

20. W. L. Kruer, Univ. of Calif. Report UCRL-82701 (May, 1979).

21. P. Kaw, G. Schmidt, and T. Wilcox. Phys. Fluids 16. 1522 (1973)

22. A. Bruce Langdon and Barbara F. Lasinski, Phys. Rev. Lett. 34, 834 (1975).

23. R. C. Malone, R. L. McCrory. and R. L. Morse. Phys. Rev. Lett. 34. 721 (1975); J. S. Pearlman and J. P. Anthes, Sandia Laboratories

24. R. R. Whitlock, F. C. Young. R. Decoste. B. H. Ripin. D. J. Nagel. J. A. Stamper, and J. M. McMachon, IEEE International Conference on Plasma Science. Austin. Texas. May 24-26. 1976.

25. B. Yaakobi and T. C. Bristow, Phys. Rev. Lett. 38, 350 (1976).

26. J. A. Stamper. K. Papadopoulos. R. N. Sudan. S. O. Dean. E. A. McLean, and J. M. Dawson, Phys. Rev. Lett., 26, 1012 (1971).

27. J. J. Thomson. C. E. Max and K. Estabrook. Phys. Rev. Lett.. 35. 663 (1975).

28. R. O. Bangerter, Univ. of Calif. Report UCRL-82274 (1979); 1978 Heavy Ion Fusion Workshop, Argonne National Laboratory, September 19-26, 1978.

29. F. Mayer and U. Reasel, J. Appl. Phys. 47. (1976); E. M. Campbell. H. G. Hicks. W. C. Mead. S. S. Glaros, L. W. Coleman, and W. B. Laird. Univ. of Calif. Report UCRL 79778 (1977).

30. W. C. Mead, J. D. Lindl, J. H. Nuckolls, J. T. Larsen, D. S. Bailey. and Y. L. Pan, Univ. of Calif. Report UCRL-80005 (1977).; European Conference on Laser Interaction with Matter, Oxford, England. Sept. 19-23. 1977.

31. V. W. Slivinsky. Univ. of Calif. Report UCRL-50021-77, p. 3-54. July. 1978.

PHYSICS OF INERTIAL CONFINEMENT PELLETS

- Overview of ICF pellet physics
- ICF driver requirements, pellet examples
- Driver/plasma coupling physics
  - Laser driver
  - Heavy ion driver
- Progress towards inertial confinement fusion

50-90-0479-1063

Fig. i

MANY COLLEAGUES HAVE CONTRIBUTED TO THE WORK PRESENTED HERE

J. H. Nuckolls
J. D. Lindl
R. O. Bangerter
A. R. Thiessen
M. D. Rosen
W. L. Kruer
K. G. Estabrook
C. E. Max
G. B. Zimmerman
D. S. Kershaw
D. S. Bailey

K. R. Manes, M. G. Boyle,
H. G. Ahlstrom, D. W. Phillion,
V. C. Rupert, et. al.

50-90-0379-0646

INERTIAL CONFINEMENT FUSION ENERGY IS RELEASED DURING TN BURN OF COMPRESSED FUEL

ICF Pellet Performance Depends on a Variety of Physical Processes

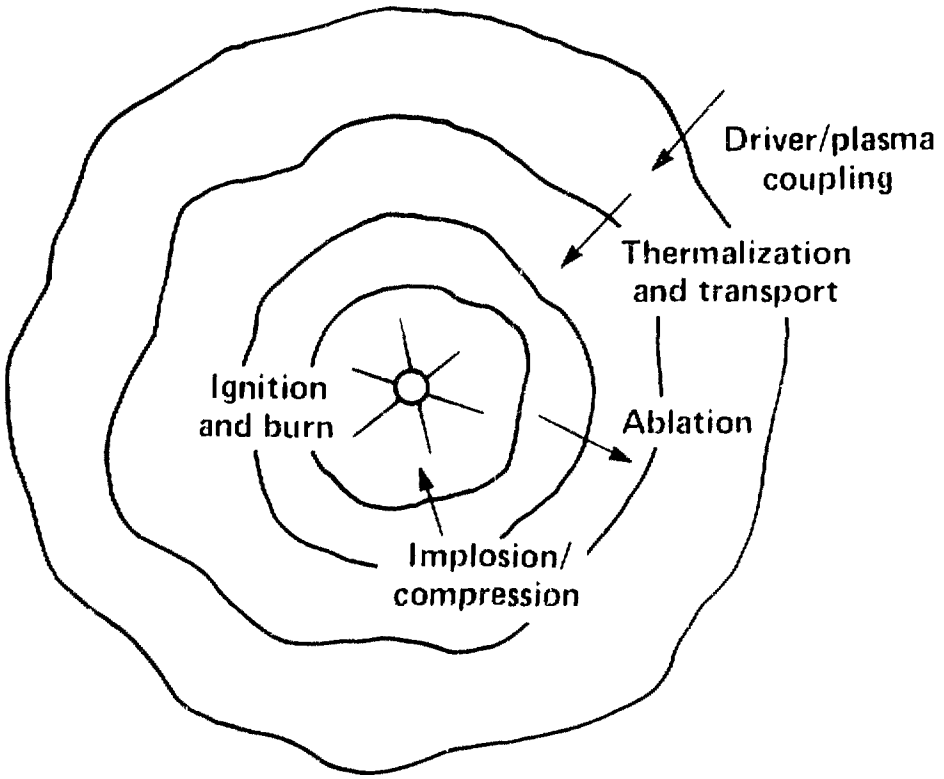

50-60-0379-0643

Fig. 1

THE SEEDS OF FUSION POWER WERE PLANTED YEARS AGO BY THE DESIGNER OF THE UNIVERSE

Get conversion of mass into energy by nuclear fusion

$$D + T \rightarrow \alpha(3.5\ MeV) + n(14.1\ MeV)$$

$$17.6\ MeV = 2.8 \times 10^{-12}\ J$$

But the seeds were well protected by the coulomb repulsion of the nuclei involved

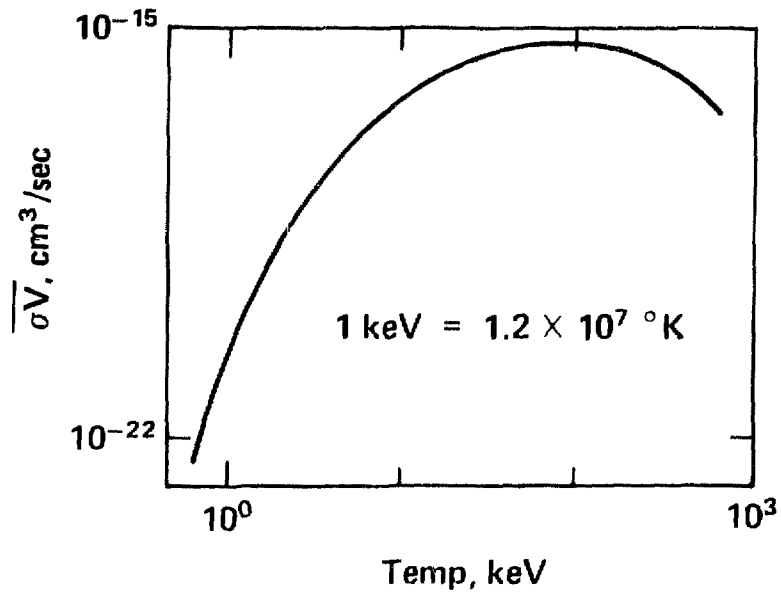

50-90-0379-0651

INERTIAL CONFINEMENT IS EFFECTIVE WHEN THE THERMONUCLEAR BURN TIME $\gtrsim$ INERTIAL DISASSEMBLY TIME

- Relative TN reaction rate in blob of DT:

$$\frac{\dot{n}_{DT}}{n_{DT}} = \frac{n_D n_T}{n_{DT}} \overline{\sigma V}(T) = \frac{A_o}{\bar{A}_{DT}} \rho_{DT} \overline{\sigma V}(T)$$

- Spherical rarefaction wave quenches burn by reducing both ρ and T:

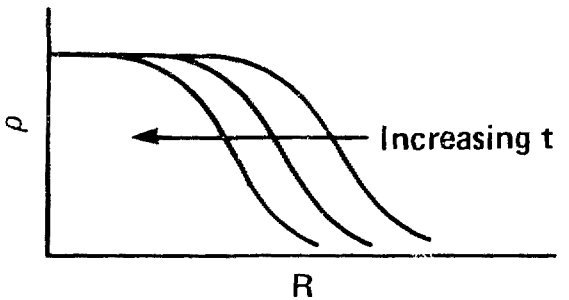

$$\tau_D \simeq \frac{R}{4c_s}$$

- Hence ρR is figure of merit for burn efficiency:

$$\phi \simeq \frac{\rho R}{\rho R + 6}$$

- Compression helps: $\rho R \propto M/R^2$

50-90-0379-0650

TN ENERGY OUTPUT FROM DT BURN CAN BE VASTLY GREATER THAN ENERGY REQUIRED TO COMPRESS IT

- Consider $\rho R = 4.5\ g/cm^2$ and $M_{DT} = 10^{-3}\ g$

  $\Rightarrow$ $\rho_{DT} = 600\ g/cm^3$ and $\phi = 40\%$

  TN energy output = $1.3 \times 10^{11}\ J/g$

- The energy invested in the fuel, assuming it can be assembled in its Fermi degenerate state is

$$\epsilon = \frac{3}{5}\epsilon_F = 3 \times 10^5\ \rho^{2/3} = 2 \times 10^7\ J/g$$

- The DT electrons will be degenerate if

$$\theta_e \ll 0.5\ \epsilon_F \simeq 0.1\ keV$$

- This is potentially terrific, but:

  1) The DT will not ignite at 0.1 keV

  and

  2) Low-isentrope compression technique is needed

50-90-0379-0649

CENTRAL IGNITION COMBINED WITH PROPAGATING BURN ARE THE KEYS TO HIGH GAIN

- DT α's have range $\rho R(g/cm^2) \simeq 0.03\ T_e$ (keV)

  or $\sim 0.3\ g/cm^2$ at $T_e = 10$ keV

- Can get central fuel region to ignite if its entropy is raised at early times such that it reaches ~10 keV when compressed to ~600 g/cm^3

  $\rho R \simeq 0.5\ g/cm^2 \Rightarrow M \simeq 1.5 \times 10^{-6}\ g \Rightarrow E_{IN} \simeq 10^3$ J at 10 keV

- Deposition of energy of α-particles from burning core sets off an outward propagating TN burn front

  $E_{OUT} \simeq 2 \times 10^4$ J; $M_{DEP} \simeq 4\pi R^2 \Delta R \rho \simeq 4 \times 10^{-6}$ g

  $\Rightarrow \epsilon \simeq 5 \times 10^9$ J/g $\Rightarrow T \simeq 40$ keV

50-90-0379-0648

SPHERICAL IMPLOSION IS THE VEHICLE REQUIRED TO DELIVER THE PHENOMENAL ENERGY DENSITY FOR ASSEMBLING INERTIALLY CONFINED FUEL

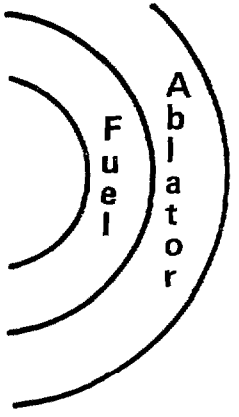

- Heating the outside of an "ablator" shell causes a pressure peak

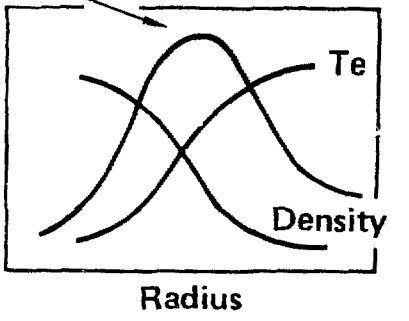

- Matter is accelerated both inward and outward by pressure gradients

- This is really an exhaust-outward spherical rocket
  Plane geometry, $m \equiv$ mass/area, $\dot{m}$ = constant

$$m(t)\ddot{r} = (m_i - \dot{m}t)\ddot{r} = P_A$$

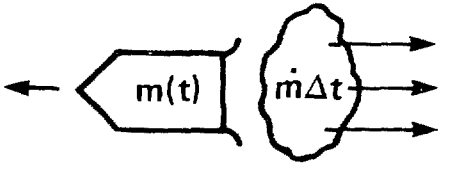

Solution

$$V(t) = \frac{P_A}{\dot{m}} \ell n \left[\frac{m_i}{m(t)}\right]$$

- Rocket gives fuel kinetic energy

50-60-0379-0641

Fig. 6

ROCKET THRUST IS DETERMINED BY HEAT FLUX DELIVERED TO ABLATION FRONT

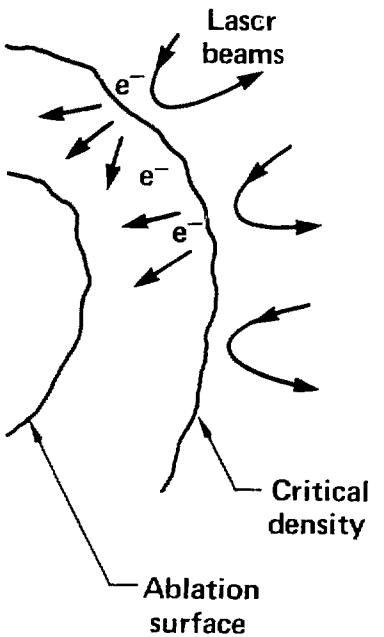

- Incident power $\dot{E}_D$ absorbed near critical density n_c w/coupling efficiency η_C

$$n_c = 1 \times 10^{21} \times (\lambda_{Nd}/\lambda_o)^2$$

- Absorbed power at critical surface, $\dot{E}_c$, plus transport flux limit, f, determine temperature, θ_c

$$\dot{E}_c = 2 \times 10^{-7}\, f n_c \theta_c^{3/2} A_c$$

$$\theta_c = 3 \times 10^{-10} \left(\frac{I_c}{f}\right)^{2/3} \left(\frac{\lambda_o}{\lambda_{Nd}}\right)^{4/3}$$

- Upon transport and thermalization, fraction η_T of total flux leaving critical surface arrives at ablation surface

$$\dot{E}_A/A_A = \eta_T \dot{E}_c/A_c$$

- Flux reaching ablation surface determines ablation pressure

$$\dot{E}_A \simeq c_A P_A A_A \text{ ; soundspeed } c_A = 3.6 \times 10^7\, \theta_A^{1/2}$$

$$P_A \simeq 1.6 \times 10^4\, f^{1/3} \left(\eta_C \eta_T I_D \frac{\lambda_{Nd}}{\lambda_D}\right)^{2/3}$$

50-60-0379-0642

WE'VE NOW GOT THE ZERO ORDER TOOLS TO COMPLETE A FIRST-CUT ICF PELLET DESIGN

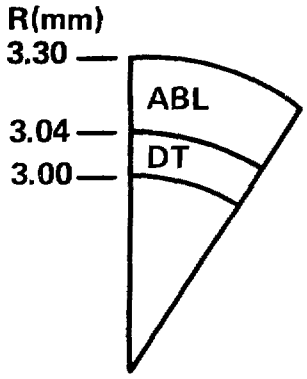

M(mg), ρ(g/cm^3)

6., 0.2

1., 0.21

- Seek final energy density of $\sim 2 \times 10^7$ J/g in fuel

$$\frac{1}{2} V_I^2 = 2 \times 10^{14} \text{ erg/g} \Rightarrow V_I = 2 \times 10^7 \text{ cm/sec}$$

- Try shell of 3 mm I.D., $\tau_I \simeq 0.3/1.0 \times 10^7 = 3 \times 10^{-8}$ sec
- Using rocket equation, find optimum kinetic energy into "payload" occurs at $m_i/m_f \simeq 7.5$

$$\dot{m} = \frac{6 \times 10^{-3}}{\pi(0.3)^2 \cdot 3 \times 10^{-8}} = 7 \times 10^5 \text{ g/cm}^2 - \text{sec}$$

- Driving pressure to attain final velocity is

$$P_A = \dot{m} V_f / \ell n \frac{m_i}{m_f} = 7 \times 10^{12} \text{ erg/cm}^3$$

- To avoid agony, assume on faith $n_c = 0.7$, $n_T = 0.5$, $f_e = 0.1$ and that we have a 0.25 μm laser sitting around; then solve transport equation to get

$I_D = 2 \times 10^{13}$ W/cm^2 peak

$\dot{E}_D \simeq 40$ TW

$E_D \simeq 0.5$ MJ

- Our reward is $\simeq$ 140 MJ of TN energy (beginner's luck!)

50-60-0379-0640

Fig. 8

TO THESE BASICS, A FEW HIGHER-ORDER CONSIDERATIONS NEED TO BE ADDED (NOT TO MENTION TECHNICAL DIFFICULTIES)

- Driver/plasma coupling may not be so simple
- Pulse shaping details are needed to set and maintain proper isentrope for fuel and ignition mass; timing is a delicate matter
- Preheat from long range particles will try to "un-degenerate" the fuel and decompress the shell
- Fluid instability may develop at the ablation surface
- Overall spherical symmetry must be maintained to permit radial convergence of ~300, requiring better than 1/2% driving pressure uniformity

50-90-0379-0647

Fig. 9

PHYSICAL CHARACTERISTICS OF PROPOSED ICF DRIVERS COVER A WIDE RANGE, INVOLVE WIDE VARIETY OF INTERACTIONS

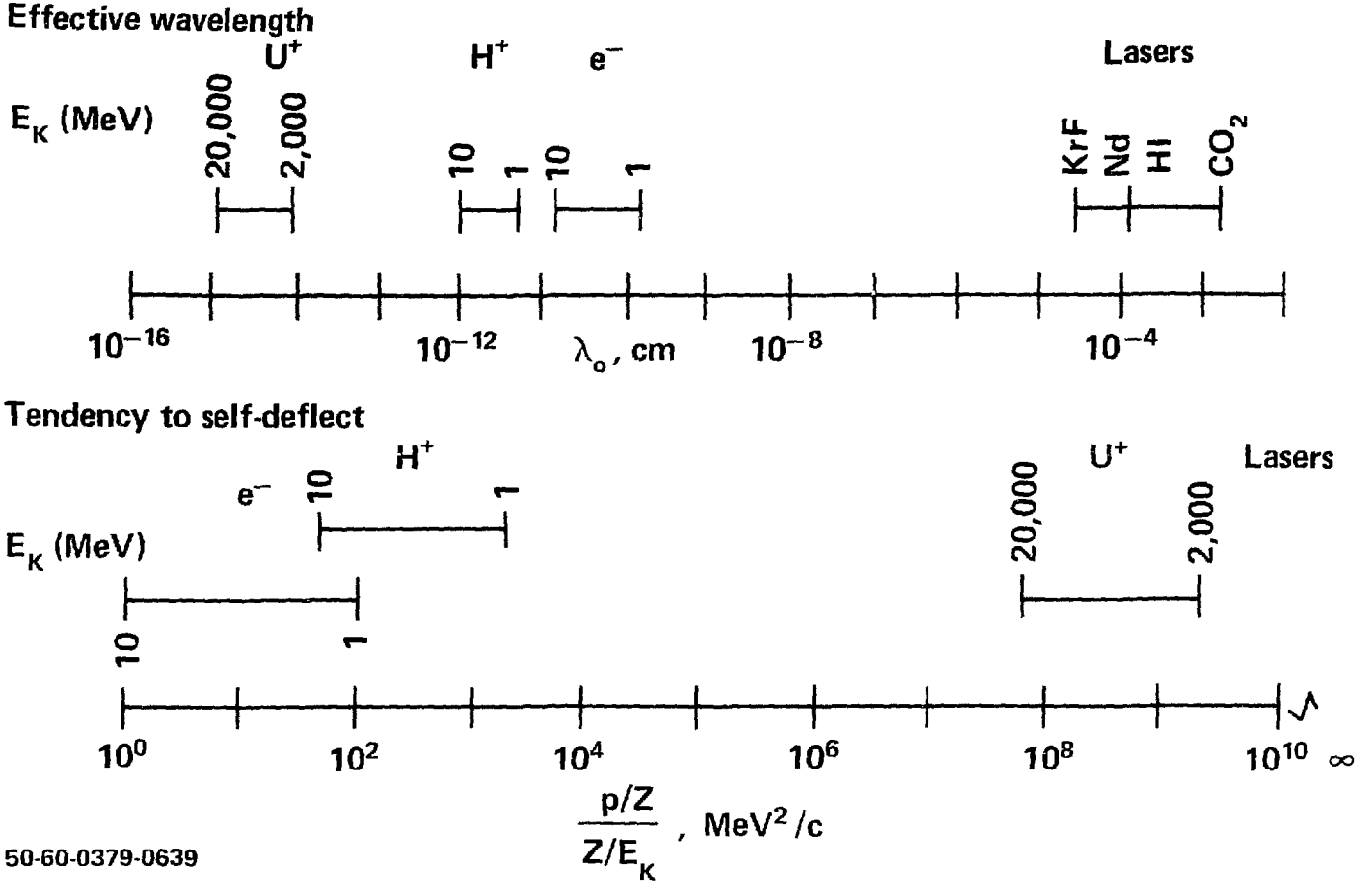

50-60-0379-0639

Fig. 10

INTERACTION RANGES OF PROPOSED ICF DRIVERS SPAN 4 ORDERS OF MAGNITUDE

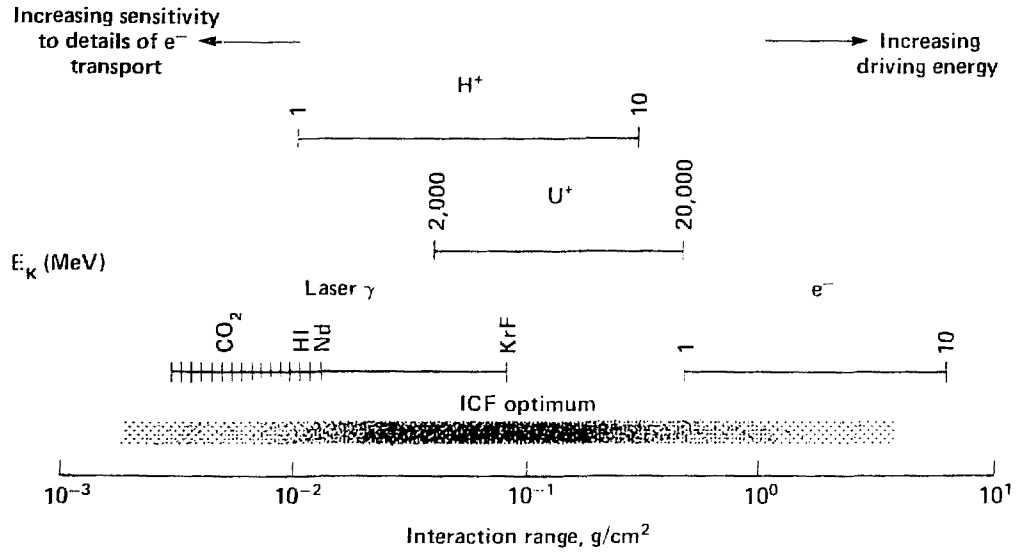

Note: Interaction range is only one aspect of driver evaluation; other factors can shift the overall optimum

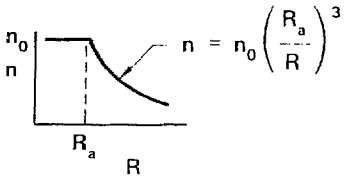

$R_a = 0.4$ cm
$A = 8$, $n_0 = 10^{23}$ cm^{-3}
$I \simeq 10^{14}$ ω/cm^2

50-60-0379-0638

Fig. 11

TO USE ICF AS A SOURCE OF COMMERCIAL ELECTRICITY, THE PRODUCT OF THE PELLET GAIN AND THE DRIVER EFFICIENCY MUST EXCEED ~ 10

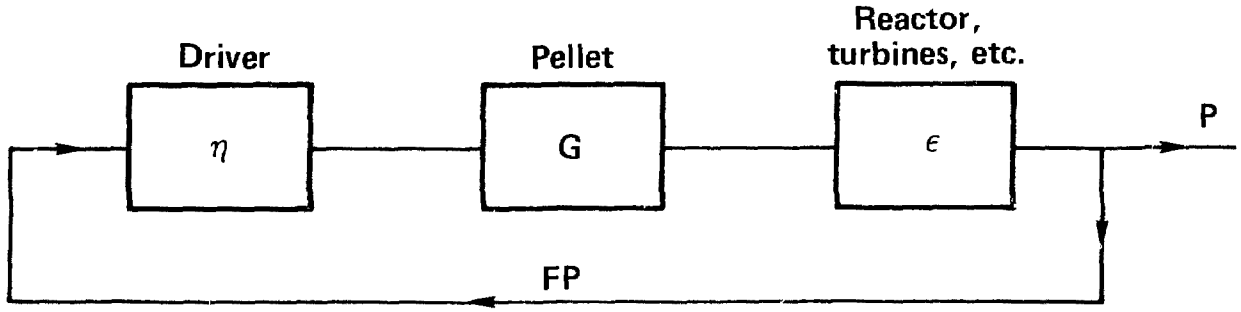

$$FP\eta G\epsilon = P + FP \qquad \eta G = \frac{1 + F}{F\epsilon}$$

$$F \lesssim 0.33, \quad \epsilon \approx 0.4 \Rightarrow \eta G \gtrsim 10$$

50-90-0379

Fig. 12

ICF DRIVER REQUIREMENTS

For ICF research facilities

Energy:	1.0 - 3.0 MJ
Power:	100 - 400 TW
Deposition characteristics:	10^7 - 10^8 J/g
Wavelength/voltage:	Limited to minimize target preheat

Additional requirements for ICF reactors

Efficiency:	1-2% [η_D Q $\geq$ 10 (driver eff. $\times$ pellet gain)]
Repetition rate:	1-20 Hz
Focusing characteristics:	must focus across 5 meters to 5 mm dia

50-60-0379-0653

Fig. 13

1 MeV e^- -BEAM SINGLE SHELL TARGET USES MASSIVE ABLATOR/ DENSE PUSHER; GAIN ~ 25 AT 6 MJ, 1200 TW

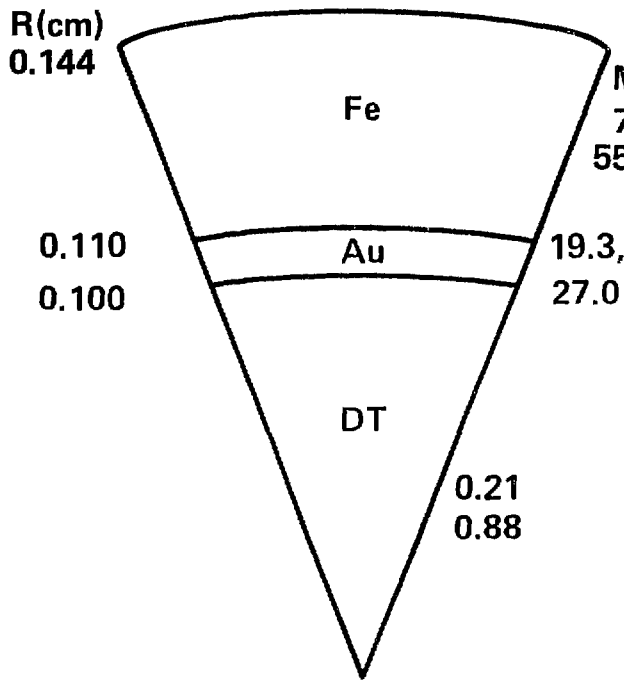

- Multiple scattering + Bremsstrahlung ⇒ broad deposition profile
- Preheat is limitation
- Long density gradients ⇒ fluid instability relatively benign

M. J. Clauser, M. A. Sweeney; D. J. Meeker

50-60-0379-0637

6.5 MeV p-BEAM DRIVEN TARGET USES "TAMPED PUSHER" TO COMPRESS FUEL; GAIN ~ 90 AT 1.3 MJ, 250 TW

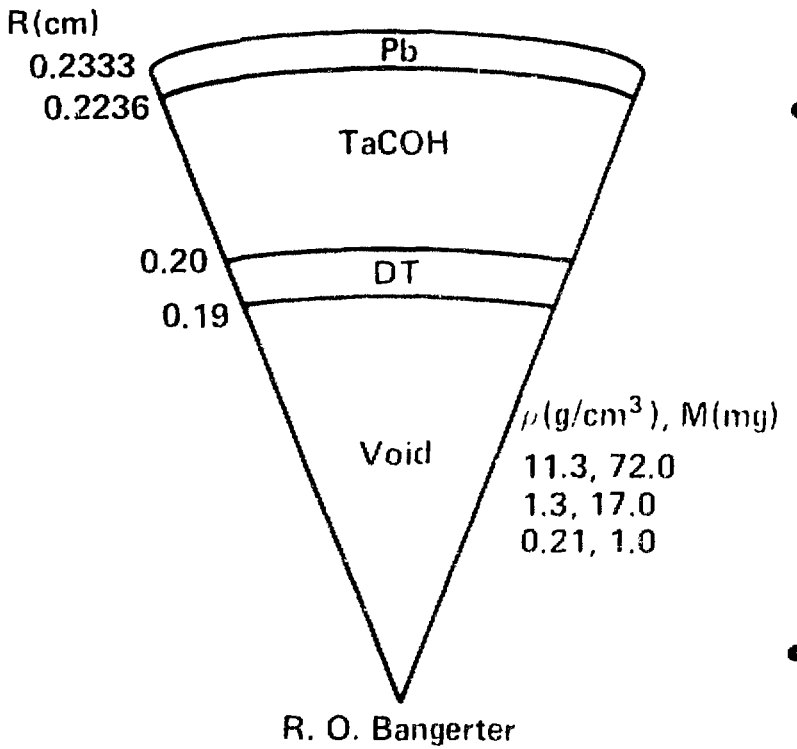

- Bragg peak in deposition rate delivers most of energy directly to pusher

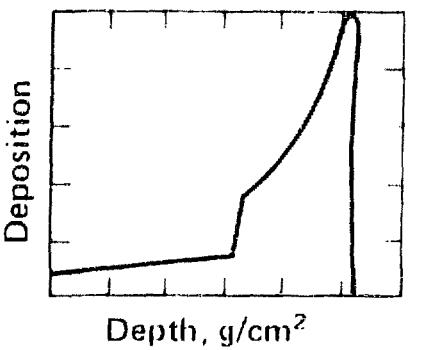

- High performance depends upon precision pulse shape

50-60-0379-0636

ABSORPTION PROCESSES DIVIDE INTO TWO GENERAL CATEGORIES

"Collisional" heating

- Inverse bremsstrahlung
- $f_{abs} \propto \nu_{ei} L \sim \nu_{ei} c_s \tau \sim \tau/\theta_e$
- Most effective at low intensity ($I \lesssim 10^{15}$ W/cm^2) and long pulse length ($\tau \gtrsim$ few hundred ps)
- Produces background (thermal) heating

"Collective" absorption

- Light wave → plasma waves → heat particles
- Dominant at high intensity and short pulse length
- In general, this heating produces a relatively small number of energetic electrons (supra-thermals)

50-60-1278-4439

Fig. 16

LASER PLASMA COUPLING IS ONE OF THE MOST CHALLENGING PROBLEMS IN LASER FUSION

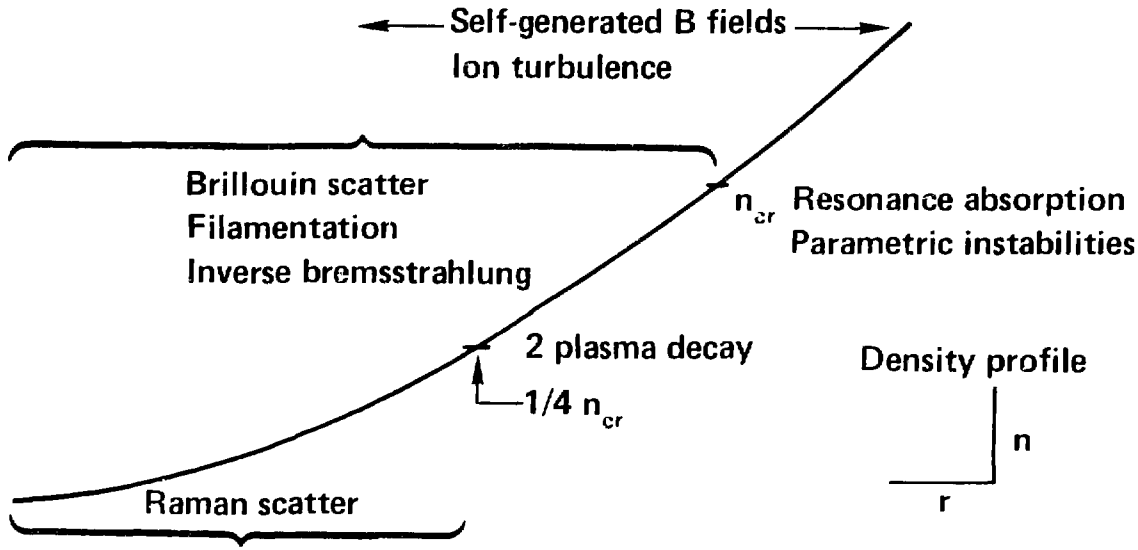

Many processes compete to determine the coupling. The mix of these processes depends on the plasma conditions. The plasma conditions depend on the mix of the processes.

50-60-1278-4445

Fig. 17

RESONANCE ABSORPTION IS THE SIMPLEST, "LOWEST ORDER" EXAMPLE OF HEATING VIA PLASMA WAVES

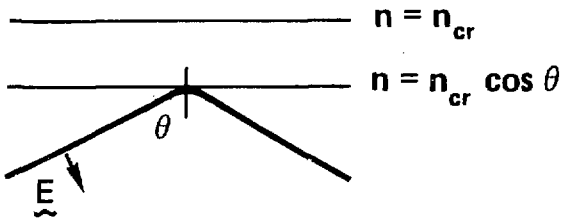

Resonance absorption

- obliquely gradient, p-polarized light
- component of its electric field oscillates electrons along the density gradient
- this imposed charge density variation resonantly drives an electron plasma wave near n_{cr}

Light and plasma wave pressure locally steepen the density profile

Calculations show typically ~ 30% absorption into hot electrons with characteristic temperature

$$\theta_h \approx 10^{-5}\ \theta_c^{0.25}\ (I_L \lambda_\mu^2)^{0.4}\ \text{keV}$$

50-60-1278-4440

THESE HOT TEMPERATURES ARE ROUGHLY WHAT ARE MEASURED FROM HIGH ENERGY X-RAY

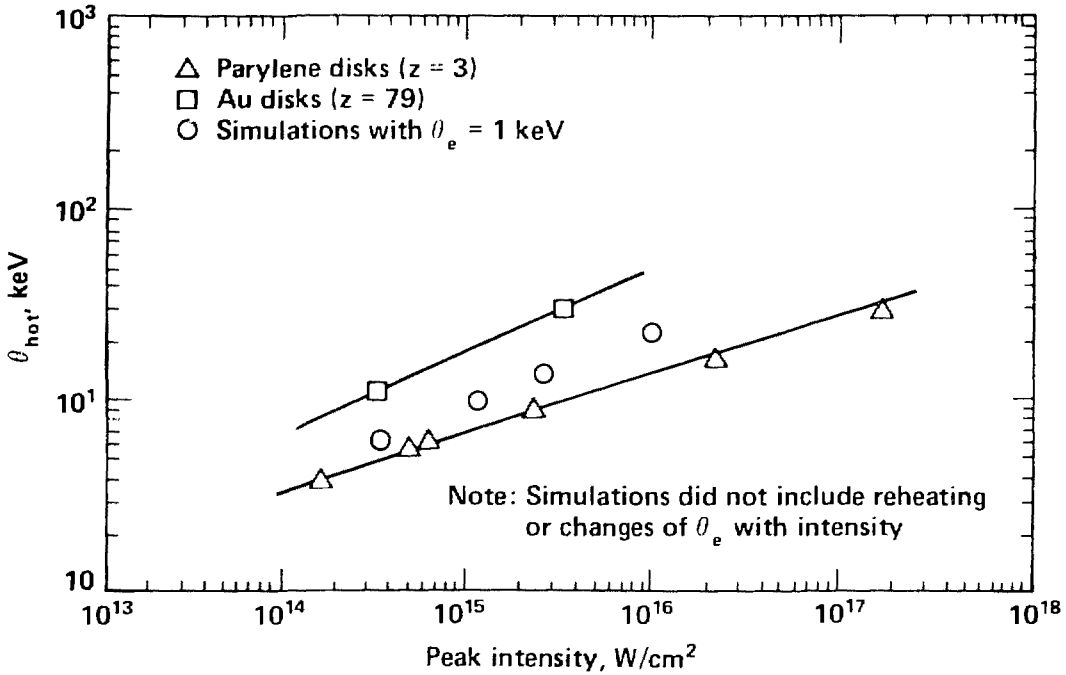

Iteration with experiments give improved numbers for target design

Note that θ_{hot} is a function of Z of the target

Note that $\theta_{hot} \sim \lambda_o^{0.8}$

50-60-1278-4441

Fig. 19

THE CALCULATIONS PREDICTED THE PRINCIPAL FEATURES OF THE ABSORPTION

- Magnitude within $\simeq$ 30%
- Polarization — dependence
- Broad angular dependence

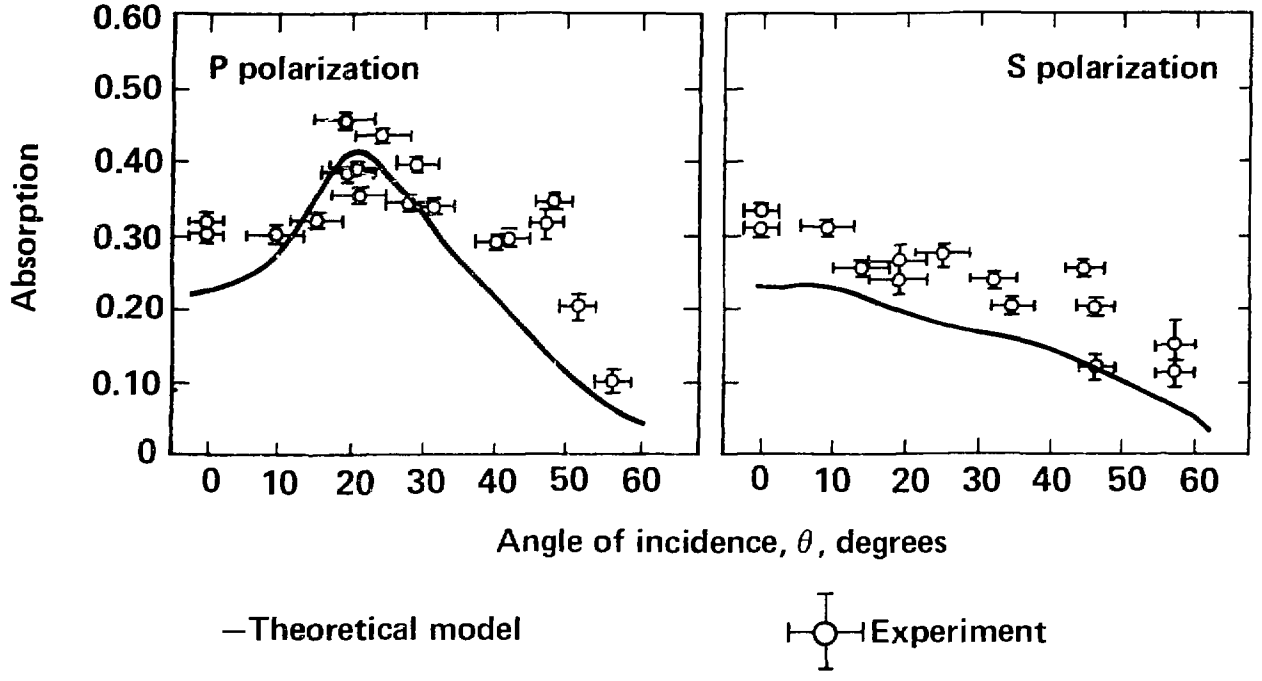

50-60-1177-2918

Fig. 20

STIMULATED BRILLOUIN SCATTERING CAN REFLECT LASER LIGHT BELOW THE CRITICAL DENSITY

SBS is produced by coupling between an incoming high frequency electromagnetic wave and a low frequency ion wave in the underdense plasma

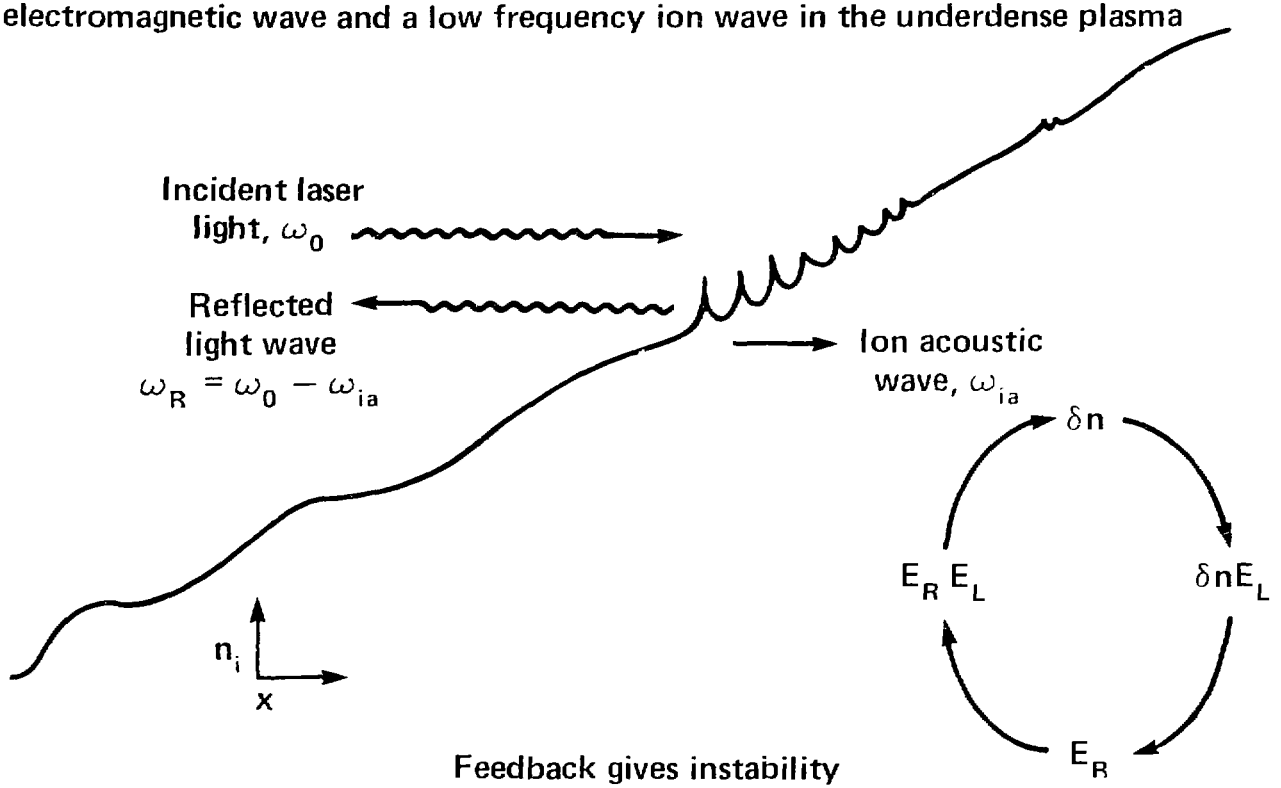

Feedback gives instability

50-60-0379-0635

Fig. 21

CALCULATIONS PREDICTED SIZEABLE BRILLOUIN SCATTER IN LONG PULSE LENGTH EXPERIMENTS

Phillion, et. al. PRL 39, 1529 (1977)

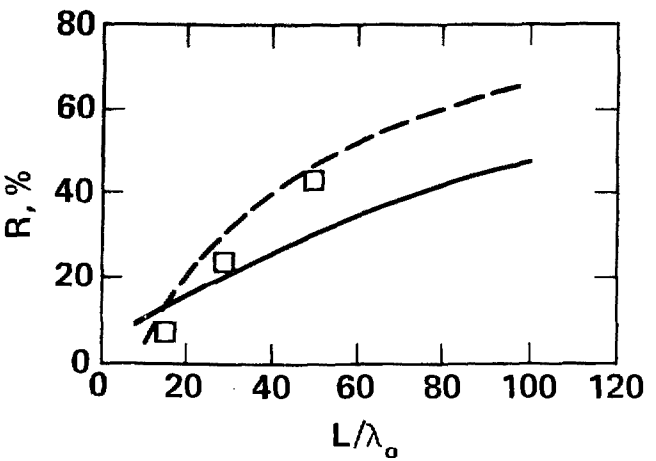

Calculations

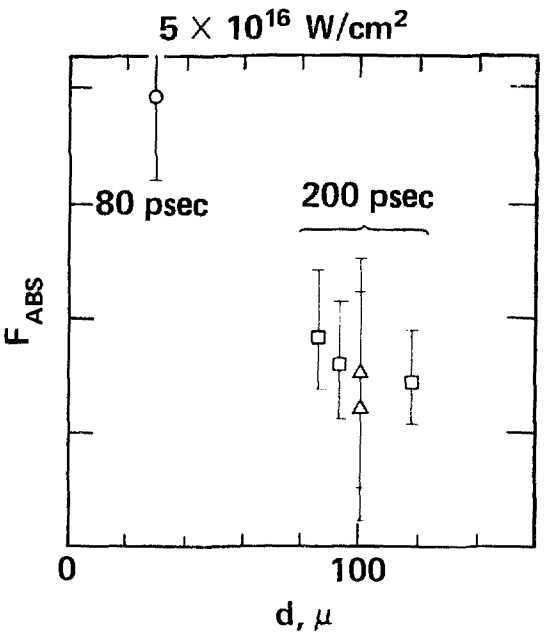

Experiments

Light is generally reflected back in a ±20-30° cone,
but can sometimes be more collimated [Ripin, et. al. PRL 39, 611 (1977)]

50-60-0379-0633

BRILLOUIN SCATTERING HEATS IONS, ION WAVES BECOME DAMPED

1-D Plasma simulation: Ion phase space
K. Estabrook

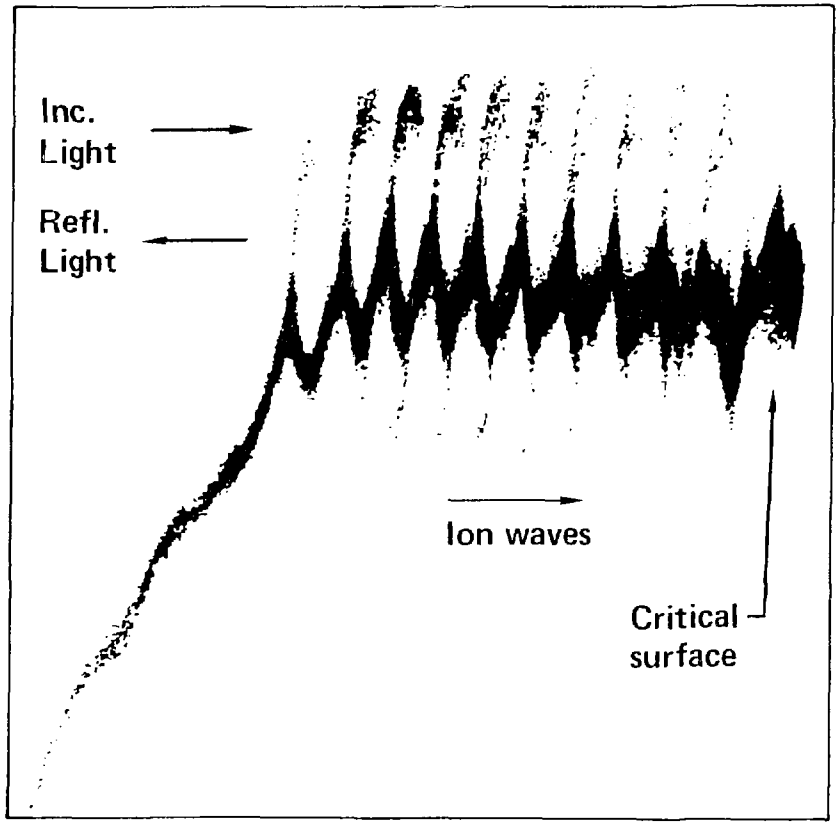

50-60-0379-0652

Fig. 23

STIMULATED BACK SCATTER CAN BE SIZEABLE IN LARGE UNDERDENSE PLASMA

Back scatter model (Kruer): $\theta_i \simeq \frac{\theta_e}{Z}$, $\nu_i \simeq \omega_i$ $\quad Q_{ss} \simeq \frac{n_p}{n_c} \left(\frac{v_{os}}{v_e}\right)^2 \frac{L}{\lambda_o}$

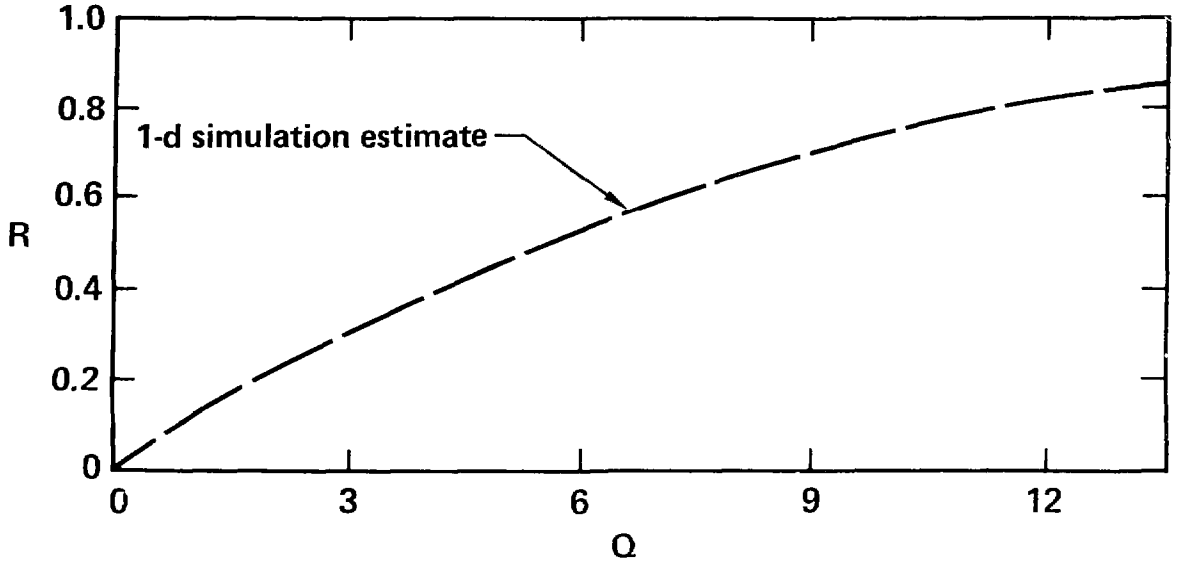

2-d simulations suggest angular spread of $\pm$ 20-30°, in agreement with some experiments

50-60-0379-0632

LASER LIGHT CAN MAKE FILAMENTS FOR LONG PULSE LENGTH, LARGE FOCAL SPOT EXPERIMENTS

- Filamentation due to ponderomotive force and due to Joule heating is above convective growth threshold, for typical parameters
  $I = 3 \times 10^{15}$ W/cm^2, $n = 0.4\ n_c$, $T_e = 10$ keV, $z = 50$

- Example: growth length of ponderomotive-force filaments for typical parameters

n/n_c	0.9	0.4	0.1
L_g/λ_0	4.0	20.0	100.0
$\ell_\perp/\lambda_0$	6.0	9.0	18.0

Best guess: growth length $\sim 20\ \lambda_0$

- Light reaches $E^2/8\pi n_c T \sim 1$ in about 30 μm (Nd, $n = 0.4\ n_c$) so at n_c, intensity will correspond to $E^2/8\pi n_c T \sim 1$, or $I \sim 5 \times 10^{16}$ W/cm^2 for typical parameters

  — Moral: can have quite high intensities at critical

50-60-0978-3244

CONSEQUENCES OF FILAMENTATION

1. Higher intensity at critical → T_{hot} increases

   $T_{hot} \sim I^{0.4}$ ⇒ factor of 3 increase in T_{hot}, for typical parameters

   ⇒ factor of 9 increase in electron range

2. Possibly more profile steepening and absorption at critical

3. $\nabla n \times \nabla T$ B fields can form around filament:

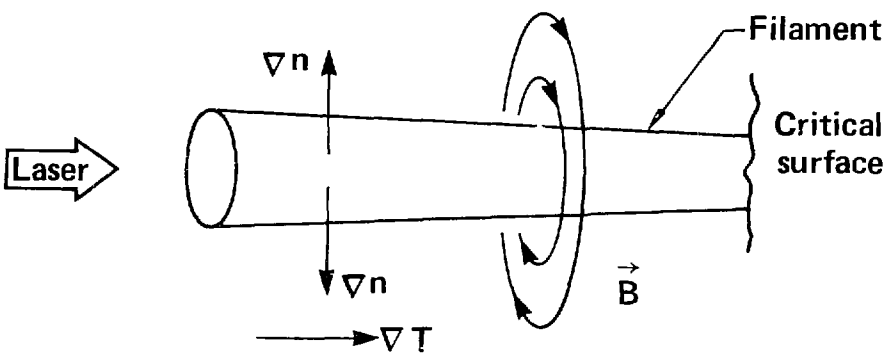

4. Hot electrons moving away from target may be channeled in this B field: $\omega_c \tau_{ei} \sim 200$, for 30 keV electrons, $n = 0.4\ n_c$, B = 1 MG, z = 50

See Donaldson and Spalding, PRL 36, 467 (1976)

50-60-0978-3245

EVIDENCE OF LOCALIZED HEATING – 1.06 μm LASER/W/GLASS DISK FILTERED X-RAY MICROSCOPE IMAGES

$I_L = 5.7 \times 10^{14}$ W/cm^2

7 μm W/glass disk

Focused laser energy distribution

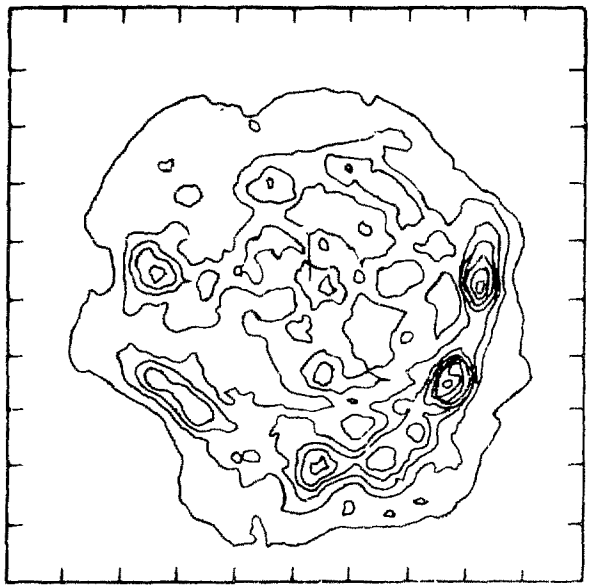

100μm

100 μm

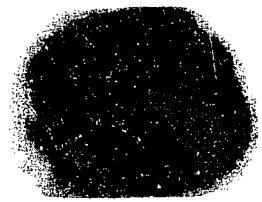

$\bar{E}_p$ = 0.8 keV

$\bar{E}_p$ = 1.5 keV

$\bar{E}_p$ = 2.5 keV

Fig. 27

ELECTRON TRANSPORT MAY BE REDUCED COMPARED WITH FREE-STREAMING VALUE IN HOT, LOW DENSITY PLASMAS

- Free streaming heat flow, $Q \sim f n_e \theta_e v_e$, $f \sim 0.5$
- Numerical modeling suggests effective flux reduction to $f \sim 0.03$ to obtain reasonable values for
  - Inverse Bremsstrahlung absorption
  - X-ray emission, spatial and spectral distributions
  - Heating depth for layered targets
- Need more quantitative understanding of
  - Return-current drag, induced $\vec{E}$-fields
  - $\nabla n \times \nabla T$ or laser-produced $\vec{B}$-fields
  - Ion turbulence

50-60-0379-0634

B FIELDS MAY PLAY A SIGNIFICANT ROLE IN TRANSPORT INHIBITION

Example $n = 2\, n_{cr}$ $\omega_{ce} = 2 \times 10^{13}$ B(MG)

$\theta_e = 1$ keV

$\theta_{hot} = 50$ keV

$Z = 25$

Cold electrons $\omega_{ce}\tau_{ei} \simeq 0.4$ B(MG) Hot electrons $\omega_{ce}\tau_{ei} \simeq 140$ B(MG)

Hence modest B fields are sufficient to inhibit hot electrons
(i.e., give $\omega_{ce}\tau_{ei} >> 1$)

Note: B fields must extend over a distance $>> r_{ce}$
$r_{ce} \simeq 6\,\mu$ for a 50 keV electron
in a 1 MG B field

50-60-0978-3271

SUMMARY OF LASER – PLASMA COUPLING

- Competition among processes very important – lead to wide variations in absorption/heating conditions
- Major phenomena:
  - Collisional absorption (low intensity)
  - Collective absorption into "hot" electrons
  - Stimulated Brillouin scatter
  - Filamentation
  - Inhibited transport
- Experiments have shown the existence of each of these
- Coupling picture generally improves at shorter λ_0 and lower intensity

50-90-0379-0645

THERE ARE TWO CLASSES OF ION-BEAM PHYSICS THAT MUST BE CONSIDERED

- Atomic
  - Electron spectrum
  - Photon production
- Nuclear
  - Charged nuclear reaction products
  - Neutrons
  - Gamma rays

50-90-0978-3423

Fig. 31

ENERGY LOSS OF IONS IN MATTER PRIMARILY RESULTS FROM BINARY COLLISIONS WITH ELECTRONS

- $$\frac{d\sigma}{d\Omega} = \frac{Z^2 e^4}{4P^2 \beta^2 \sin^4 \frac{\theta}{2}} \left(1 - \beta^2 \sin^2 \frac{\theta}{2}\right)$$

(Mott cross section)

- Electron kinetic energy = $T = m\beta^2 \gamma^2 (1 - \cos\theta)$

- $$\frac{d\sigma}{dT} = \frac{2\pi Z^2 e^4}{m\beta^2} \left[\frac{1}{T^2} - \frac{1}{2m\gamma^2 T}\right] \sim \frac{A}{T^2}$$

50-60-0978-3420

THE ENERGY LOSS OF AN ION IS CALCULATED BY INTEGRATING $d\sigma/dT$ OVER APPROPRIATE LIMITS

- $\frac{dE}{dx} \propto \frac{Z^2}{\beta^2} \ln \frac{T_{max}}{T_{min}}$
- $T_{max} = 2m\beta^2\gamma^2 =$ 180 keV for 20 GeV uranium (stops in ~ 1 ps at $\rho = 1$)
- $T_{min} \sim$ binding energy for atomic electrons
- T_{min} determined by debye length for plasmas
- $\frac{dE}{dx} \propto \frac{Z^2}{\beta^2} \left(\ln \frac{2m_e \beta^2 \gamma^2}{\langle I \rangle} + G\left(\frac{V_i}{V_e}\right) \ln \Lambda \right)$ + ionic loss

50-60-0978-3419

Fig. 33

ONE CAN PLACE A RIGOROUS LOWER LIMIT ON T_{max}/T_{min}

- $T_{max} = 2m_e(\beta\gamma)^2 \sim 100$ keV

  $T_{min} = \dfrac{2Z^2e^4}{mc^2\beta^2\lambda_d^2} \lesssim 10^{-2}$ keV

  Only a few electrons/λ_d^3 so collisions binary out to λ_d.

- For plasma excitation multiply T_{max}/T_{min} by $[1.123\,\beta c/\omega_p\lambda_d]^2 \sim 290$

- Binary collisions account for

  $\ell n\ 10^4/\ell n\ (290 \times 10^4) = 62\%$ of total

50-90-0479-1062

Fig. 34

A LOWER LIMIT ON dE/dx CAN BE DERIVED FROM THREE "SIMPLE" ASSUMPTIONS

- Validity of Mott cross section
- Weak dependence of Z_{eff} on target conditions (for relevant beam and target parameters)
- Binary nature of collisions for impact parameters Less than λ_d (only a few electrons per λ_d^3).

50-90-0479-1061

Fig. 35

ELECTRIC FIELDS THAT COULD ALTER dE/dx FOR HEAVY IONS ARE ENERGETICALLY IMPOSSIBLE

- Fields would have to be $E \sim 10^8$ V/cm over about 1 cm
- Joule heating gives power dissipation of E^2/η
- Spitzer resistivity gives $\eta \sim 10^{-3}$ ohm-cm for high Z

  $\eta \sim 10^{-5}$ ohm-cm for low Z
- $E = 2 \times 10^8$ V/cm gives $\gtrsim 10^{19}$ W/cm^3 in high Z and

  $\gtrsim 10^{21}$ W/cm^3 in low Z
- Beam deposition is only $\lesssim 3 \times 10^{15}$ W/cm^3

50-90-0479-1060

HEAVY ION FUSION BEAMS ARE NOT TRULY "INTENSE" IN TARGET

- Typical beam parameters

  Kinetic energy $\sim$ 10 GeV, $\beta \sim 0.3$

  Power $\sim 10^{14}$ watts

  Beam radius $\gtrsim$ 1 mm

  $n_b \sim 10^{14}/cm^3$

- Typical target parameters

  $n_e \sim 10^{23}/cm^3$ ($\sim$ solid density)

  $\theta \sim$ 200 eV

  $\lambda_d \sim 3 \times 10^{-8}$ cm

  $\beta_e \sim 0.03$

- There are $\sim 10^{13}$ debye lengths between ions and $n_e/n_b \sim 10^9$

50-90-0479-1059

Fig. 37

ELECTRON PREHEAT IS NOT A PROBLEM FOR HEAVY ION FUSION

- $E_e = 4E_I \frac{M_E}{M_I} \sim 10^{-5} E_I$
- $R_e < 0.8 E_e$
- $R_I \sim 2 \times 10^{-5} E_I$
- $R_e < R_I$
- Monte Carlo calculations confirm this result for non-radial incidence

50-90-0479-1058

NUCLEAR INTERACTIONS REPRESENT WASTED ENERGY BUT ARE NOT A FUNDAMENTAL PROBLEM

- Fraction of nuclei that survive = $\exp\left(\frac{-R(g/cm^2)\,\sigma(mb)}{1673\ A_{target}}\right)^{**}$

$$\sigma = 50\left[A_{beam}^{1/3} + A_{target}^{1/3} - 0.4\right]^2$$

- For 20 GeV uranium in Be, $R \approx 0.33\ g/cm^2$,
  $\sigma = 3100$ mb $\Rightarrow$ 93% survive

**Silberberg & Tsao

50-90-1078-3471

MEASUREMENTS AGREE WITH CALCULATIONS

Ion	Target	Energy/nucleon, MeV	Measured range, g/cm^2	Calculated
Ar	H_2O	500	12.7	13.4
Fe	Al	600	15.4	16.5
Fe	Pb	600	23.4 (23.371 ± 0.062)	27.4 (24.42 ± 0.18)
Ar	Ar	10	0.0055	0.0055
			(10 to 8 MeV/nucleon)	

Measurements have not been made in exactly relevant regime:

5 GeV U^+

"Warm" plasma

$\sim 10^4$ W/cm^2

50-90-0479-1056

Fig. 40

SUMMARY OF HEAVY-ION/PLASMA COUPLING

- Theory for cold matter well established
- Rigorous upper limit on ion range is low enough to permit use of 5-10 GeV U to drive ICF targets
- Preheat from heated electrons and nuclear reaction losses both appear tolerable

50-90-0379-0644

Fig. 41

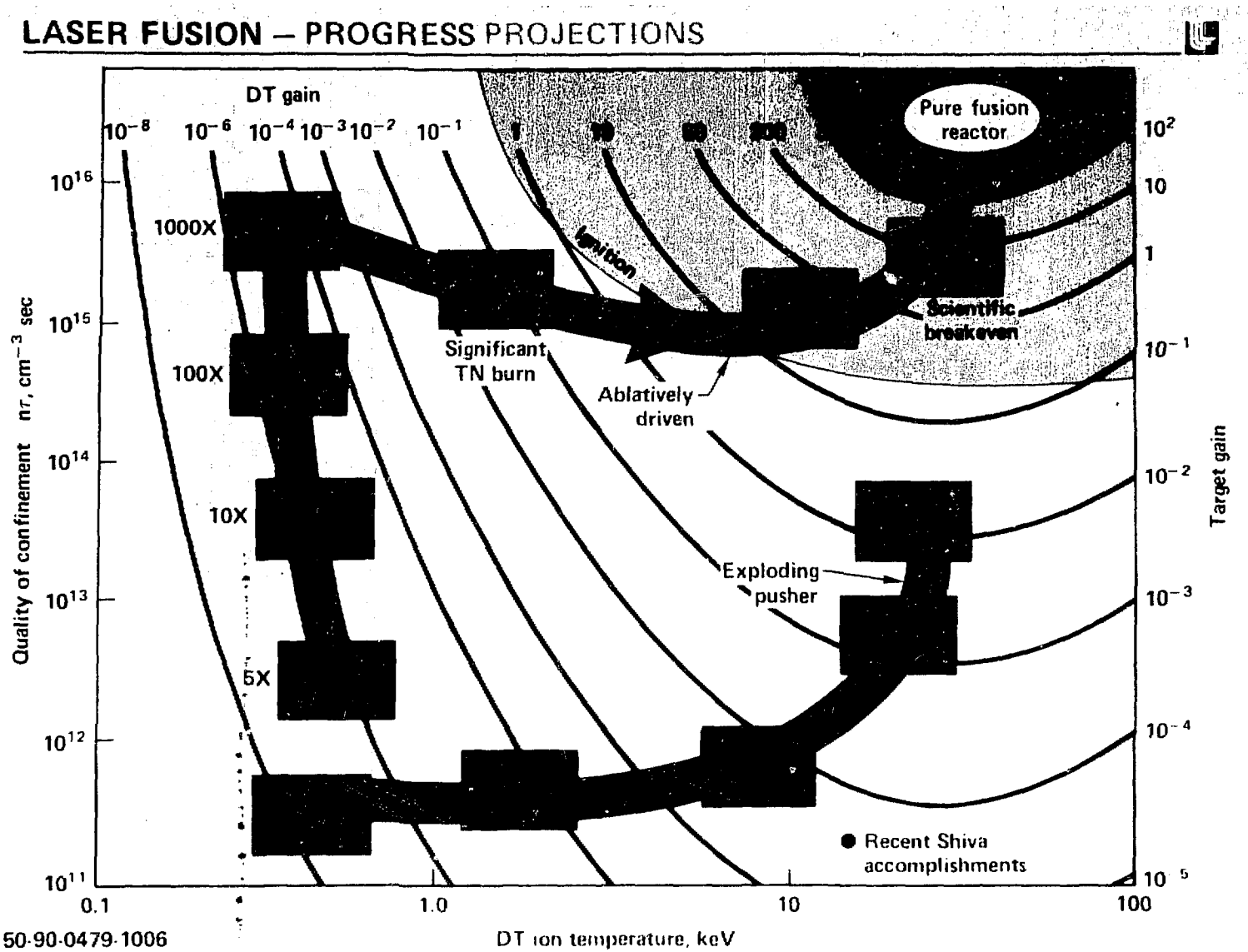
LASER FUSION – PROGRESS PROJECTIONS
DT gain
10^{-8} 10^{-6} 10^{-4} 10^{-3} 10^{-2} 10^{-1} 1 10 50 200
Pure fusion reactor
Ignition
Scientific breakeven
1000X
100X
10X
5X
Significant TN burn
Ablatively driven
Exploding pusher
Recent Shiva accomplishments
Quality of confinement nτ, cm^{-3} sec
10^{16}
10^{15}
10^{14}
10^{13}
10^{12}
10^{11}
10^{2}
10
1
10^{-1}
10^{-2}
10^{-3}
10^{-4}
10^{-5}
Target gain
0.1
1.0
10
100
DT ion temperature, keV
50-90-0479-1006

Fig. 42

NUCLEAR ACTIVATION OF PUSHER MATERIAL PROVIDES $\overline{\rho r}$ MEASUREMENT DURING BURN, CAN INFER FUEL DENSITY

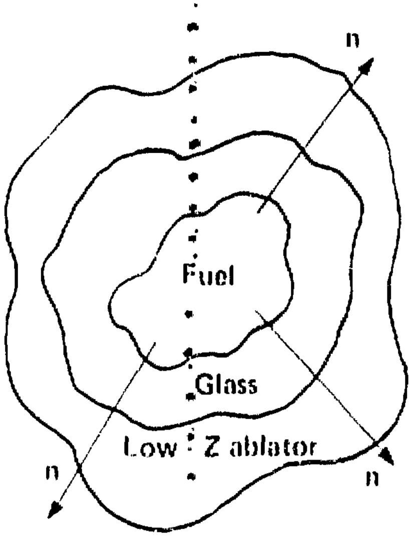

- Activation, yield $\propto \rho R)_{PUSHER}$

$n + {}^{28}Si \rightarrow {}^{28}Al + p$

$\sigma = 0.25$ b

${}^{28}Al \rightarrow {}^{28}Si^{*} + \beta^{-}$ → γ

Measure neutron yield, Y
Collect debris
Coincidence count activations, A
$\eta = \eta_{COLL}\,\eta_{DET}\,\eta_{DEC}$

$$\rho R)_{PUSHER} = \frac{A}{2.1 \times 10^{-3}\,\eta Y}$$

- Model relates pusher ρR to fuel density

Simplest form, thin shells at constant density, 1-d

Assume instantaneous burn at peak density

$$M_f^G = \eta_p M_i^G$$

$$\rho_f^{DT} = \left[\frac{(\rho R)_f^G}{\eta_p (\rho R)_i^G}\right]^{\frac{3}{2}} \rho_i^{DT}$$

10^6 n, ρr ≈ 0.02 g/cm^2

→ 75 activations

Implosion model to calculate η_p

Cleanest result when $\eta_p \approx 1$

50-60-0379-0631

TWO METHODS ALLOW DENSITY DETERMINATION USING Ar SEED IN FUEL

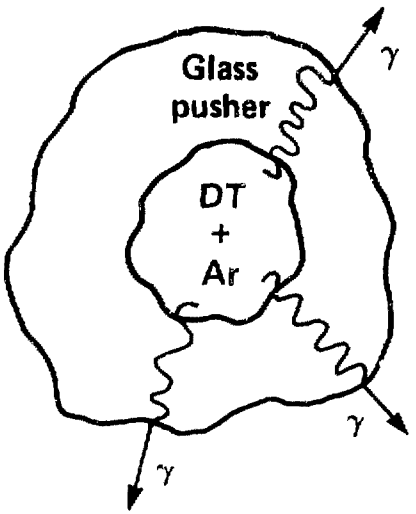

H-, He- like Ar
resonance
line emission

- Lorentz broadening
  - High resolution spectrograph
    - $10\ g/cm^3 \Leftrightarrow 3\ eV$ width
  - Doppler broadening must not dominate
    - $T_e < 700\ eV$
- Emission region diameter measurement
  - Low energy dispersion spectrograph
  - Source size determines recorded line width
    - $\Delta h\nu < 5\ eV \Leftrightarrow 7\ \mu m$ spatial resolution

50-60-0379-0630

ALTHOUGH ICF FEASIBILITY IS NOT YET ESTABLISHED, PROGRESS IN TARGET, DIAGNOSTIC, LASER, EXPERIMENT AND THEORY HAS BEEN SIGNIFICANT

Summary of Results: LLL, LASL, KMSF, LLE, NRL

- Wide range of interaction experiments showing
  - Existence and characteristics of some of the major laser/plasma interaction phenomena
  - Increasingly quantitative theoretical understanding & modeling
- Implosion experiments have shown
  - Successful compression and nuclear reaction at λ = 0.5, 1.06, 10.6 μ
  - Demonstration of TN burn via ion temperature measurement
  - Fusion yields to 3×10^{10} neutrons (1.06 μ, 20 TW), 1×10^{8} neutrons (10.6 μ, 5 TW)
  - Compression of DT to 10 g/cc final density on moderate isentrope
  - Generation of 5000 Mb peak pressure

50-90-0479-1051

Fig. 45